

SCIENTIFIC REPORTS



OPEN

Surface mechanomyography and electromyography provide non-invasive indices of inspiratory muscle force and activation in healthy subjects

Manuel Lozano-García^{1,2,3}, Leonardo Sarlabous^{1,2,3}, John Moxham⁴, Gerrard F. Rafferty^{5,6}, Abel Torres^{1,2,3}, Raimon Jané^{1,2,3} & Caroline J. Jolley^{5,6}

The current gold standard assessment of human inspiratory muscle function involves using invasive measures of transdiaphragmatic pressure (P_{di}) or crural diaphragm electromyography (oesEMG_{di}). Mechanomyography is a non-invasive measure of muscle vibration associated with muscle contraction. Surface electromyogram and mechanomyogram, recorded transcutaneously using sensors placed over the lower intercostal spaces (sEMG_{ic} and sMMG_{ic} respectively), have been proposed to provide non-invasive indices of inspiratory muscle activation, but have not been directly compared to gold standard P_{di} and oesEMG_{di} measures during voluntary respiratory manoeuvres. To validate the non-invasive techniques, the relationships between P_{di} and sMMG_{ic} and between oesEMG_{di} and sEMG_{ic} were measured simultaneously in 12 healthy subjects during an incremental inspiratory threshold loading protocol. Myographic signals were analysed using fixed sample entropy (fSampEn), which is less influenced by cardiac artefacts than conventional root mean square. Strong correlations were observed between: mean P_{di} and mean fSampEn |sMMG_{ic}| (left, 0.76; right, 0.81), the time-integrals of the P_{di} and fSampEn |sMMG_{ic}| (left, 0.78; right, 0.83), and mean fSampEn oesEMG_{di} and mean fSampEn sEMG_{ic} (left, 0.84; right, 0.83). These findings suggest that sMMG_{ic} and sEMG_{ic} could provide useful non-invasive alternatives to P_{di} and oesEMG_{di} for the assessment of inspiratory muscle function in health and disease.

The ability to measure respiratory muscle function is clinically important in the assessment of neuromuscular¹ and respiratory disease². In the respiratory system, respiratory muscle force is usually estimated as pressure, and shortening as lung volume change or displacement of chest wall structures³. Moreover, respiratory muscle force is tightly related to the level of activation of the muscles^{3,4}, which can be assessed by electromyography. The diaphragm is the main inspiratory muscle^{5,6}, and so it is important to be able to measure diaphragm function accurately. Accurate assessment of diaphragm pressure generation and activation, however, requires invasive procedures, such as the balloon-catheter technique, to measure transdiaphragmatic pressure (P_{di})⁷, or crural diaphragm electromyography using a multipair oesophageal electrode (oesEMG_{di})^{2,8-10}. These invasive tests can be uncomfortable for patients and require some skill from the operator involved. They are therefore rarely carried out in clinical practice. The development of novel, non-invasive indices of diaphragm force output and activation

¹Biomedical Signal Processing and Interpretation group, Institute for Bioengineering of Catalonia (IBEC), The Barcelona Institute of Science and Technology (BIST), Barcelona, Spain. ²Biomedical Research Networking Centre in Bioengineering, Biomaterials and Nanomedicine (CIBER-BBN), Barcelona, Spain. ³Department of Automatic Control (ESAI), Universitat Politècnica de Catalunya (UPC)-Barcelona Tech, Barcelona, Spain. ⁴Faculty of Life Sciences & Medicine, King's College London, King's Health Partners, London, United Kingdom. ⁵King's College Hospital NHS Foundation Trust, King's Health Partners, London, United Kingdom. ⁶Centre for Human & Applied Physiological Sciences, School of Basic & Medical Biosciences, Faculty of Life Sciences & Medicine, King's College London, King's Health Partners, London, United Kingdom. Raimon Jané and Caroline J. Jolley contributed equally. Correspondence and requests for materials should be addressed to M.L.-G. (email: mlozano@ibecbarcelona.eu)

would therefore represent a significant advance in the assessment of patients with disordered respiratory muscle function.

Transcutaneous assessment of muscle fibre vibration during contraction provides the opportunity to non-invasively quantify an index of the force exerted by the underlying contracting skeletal muscle¹¹. In common with other skeletal muscles¹¹, diaphragm muscle fibres vibrate laterally during contraction¹². These vibrations, related to the mechanical activation of diaphragm muscle fibres, can be non-invasively recorded as sound, using microphones (phonomyography), to provide a non-invasive index of electromechanical coupling, recruitment, and P_{di} generation by the diaphragm¹². Alternatively, inspiratory muscle fibre vibration can be recorded by mechanomyography, using skin-surface accelerometers positioned on the chest wall over the lower intercostal spaces, proximal to the zone of apposition of the diaphragm (sMMG_{lic})^{13–15}. The surface mechanomyogram (sMMG) is considered to be the mechanical counterpart of motor unit (MU) electrical activity as measured by surface electromyography (sEMG)¹⁶, and confers several important advantages. Unlike sEMG, sMMG is not influenced by skin preparation, bioelectrical interference from other muscles or by power line interference. Despite this, the use of sMMG to assess inspiratory muscle function has been relatively unexplored, and sMMG_{lic} has not been compared with gold standard invasive measures of P_{di} , during voluntary respiratory manoeuvres.

Measurements of both sEMG_{lic} and sMMG_{lic} are, however, contaminated by cardiac artefacts, especially using the average rectified value or root mean square (RMS) as standard. Recently, fixed sample entropy (fSampEn) has been proposed as a means to estimate the respiratory muscle effort from sMMG_{lic}^{13,14} and sEMG_{lic}¹⁷ signals, with less interference from cardiac artefacts. However, fSampEn has not previously been applied to analysis of gold standard invasive oesEMG_{di} measures.

The principal aim of the study was, therefore, to investigate the use of sMMG_{lic} as a novel non-invasive index of inspiratory muscle force, by examining its relationship with the invasive gold standard, P_{di} , in healthy subjects during an incremental inspiratory threshold loading protocol. We hypothesized that there would be close positive linear relationships between mean fSampEn |sMMG_{lic}| and mean P_{di} , and between the time-integrals of these signals. The relationship between invasive oesEMG_{di} and non-invasive sEMG_{lic} was also investigated. In addition, we aimed to compare the utility of RMS- and fSampEn-based techniques to analyse oesEMG_{di} signals, hypothesizing that there would be a close positive relationship between RMS- and fSampEn-derived measures of oesEMG_{di}.

Experimental

Ethical approval. This study was approved by the NHS Health Research Authority (NRES Committee London – Dulwich 05/Q0703) and the experiments conformed to the standards of the Declaration of Helsinki. All subjects were fully informed of any risk associated with the study and provided their written consent before participation.

Subjects. Adult subjects, familiar with physiological studies, with no history of cardiorespiratory or neuromuscular disease were recruited.

Measurements. Both invasive and non-invasive measurements of inspiratory muscle force and activation were obtained simultaneously from all subjects. Unless specified, all measures were recorded continuously during all stages of the protocol.

Invasive measurements. P_{di} was measured as the difference between gastric and oesophageal pressure obtained using a dual-pressure transducer tipped catheter (CTO-2; Gaeltec Devices Ltd., Dunvegan, UK) and associated amplifier (S7d; Gaeltec Devices Ltd., Dunvegan, UK), as previously described^{18–20}.

Crural oesEMG_{di} was recorded using a multipair oesophageal electrode catheter (Yinghui Medical Equipment Technology Co. Ltd., Guangzhou, China). The catheter consisted of nine consecutive recording electrode coils, which formed five pairs of electrodes^{2,21}. The pressure transducer and electrode catheters were inserted transnasally and once correctly positioned, taped to the nose to prevent movement during the study.

Non-invasive measurements. sMMG_{lic} was recorded using two triaxial accelerometers (TSD109C2; BIOPAC Systems Inc., CA, USA), and associated interface (HLT100C) and isolated power supply (IPS100C) modules (BIOPAC Systems Inc., CA, USA). The accelerometers were attached bilaterally to the skin with adhesive rings as close as possible to the surface EMG electrodes along the seventh or eighth intercostal space, over the anterior axillary line¹⁴.

sEMG_{lic} was recorded bilaterally using two pairs of disposable surface Ag/AgCl electrodes (H124SG; Covidien Kendall) placed on the skin over the seventh or eighth intercostal spaces, between the mid-axillary and the anterior axillary lines^{8,12,17,22}. Electrode pairs were spaced 2 cm apart and a ground electrode was placed on the clavicle. The skin was appropriately prepared prior to electrode application.

Respiratory airflow was measured using a pneumotachograph (4830; Hans Rudolph Inc., KS, USA) connected to a differential pressure transducer (DP45; Validyne Engineering, CA, USA) and amplifier (CD72; Validyne Engineering, CA, USA). Mouth pressure (P_{mo}) was measured from a side port on the pneumotachograph using a second differential pressure transducer (MP45; Validyne Engineering, CA, USA) attached to the amplifier.

Signal Acquisition. The oesEMG_{di} and sEMG_{lic} signals were amplified (gain 100), high-pass filtered at 10 Hz, and AC-coupled before acquisition (CED 1902; Cambridge Electronic Design Limited, Cambridge, UK). All signals were acquired using a 16-bit analogue-to-digital converter (PowerLab 16/35; ADInstruments Ltd., Oxford, UK) and displayed on a laptop computer running LabChart software (Version 7.2, ADInstruments Pty, Colorado Springs, USA) with analogue to digital sampling at 100 Hz (flow and pressures), 2000 Hz (sMMG_{lic}), and 4000 Hz (oesEMG_{di} and sEMG_{lic}).

Maximal volitional manoeuvres. Three maximal volitional inspiratory manoeuvres were performed initially: maximal static inspiratory pressure from functional residual capacity³ (P_{Imax}), maximal sniff pressure, and maximal inspiration to total lung capacity^{2,9}. These manoeuvres were performed sitting upright in a chair with a noseclip in place (except for maximal sniffs) and were repeated several times to ensure maximal volitional effort. P_{di}, oesEMG_{di}, sEMG_{lic}, and sMMG_{lic} were recorded continuously during the manoeuvres and peak values determined for subsequent normalization of oesEMG_{di} recorded during the inspiratory loading protocol (see below). Each participant's P_{Imax} value was used to determine the inspiratory threshold loads used in their individual incremental inspiratory threshold loading protocol.

Inspiratory threshold loading protocol. All participants performed an inspiratory threshold loading protocol at five inspiratory threshold loads set at 12% (L1), 24% (L2), 36% (L3), 48% (L4), and 60% (L5) of the subject's P_{Imax}. Inspiratory threshold loads were generated using an electronic inspiratory muscle trainer (POWERbreathe K5; POWERbreathe International Ltd., Southam, UK) attached to the distal end of the pneumotachograph. The inspiratory muscle trainer had an electronically controlled resistance valve that provided a pressure threshold resistance, which was set using the associated software (Breathe-Link, POWERbreathe International Ltd., Southam, UK). Subjects were seated and breathed through the pneumotachograph via a mouthpiece with a noseclip in place. Baseline measurements were recorded during a minimum of 2 minutes of quiet tidal breathing, following which the inspiratory muscle trainer was attached to the pneumotachograph and the series of threshold loads was imposed. Subjects were not provided with any specific instructions to adopt a certain duty cycle, and were free to choose their own breathing frequency. Subjects were, however, informed that effort was needed to overcome the threshold loads, and they were therefore encouraged to focus on using their diaphragm, to perform quick deep inspirations and to ensure that expiration was complete before making their next inspiratory effort. Each load consisted of 30 breaths followed by a resting period to allow all objective and subjective respiratory measures to return to baseline. Participants were asked to score breathlessness intensity at the end of each load using the modified Borg scale (mBorg)²³. Participants were coached to anchor responses to mBorg 0 (no breathlessness), mBorg 10 (maximum breathlessness intensity imaginable) and mBorg 5 (severe, half maximal).

Data analysis. LabChart data were exported as Matlab files, and analysed offline in the widely available Matlab R2014a software. All signal processing and data analysis procedures described below were automated.

Signal filtering and pre-processing. sMMG_{lic} signals were resampled at 200 Hz and filtered with a 4th-order zero-phase Butterworth band-pass filter between 5 and 35 Hz. Each accelerometer simultaneously provided three sMMG_{lic} signals (sMMG_{lic} X, sMMG_{lic} Y, and sMMG_{lic} Z), representing acceleration of muscle fibre vibration along all three spatial directions. A new signal, representing the total acceleration of muscle fibre vibration measured by each accelerometer, was arithmetically calculated as the norm of the vector formed by the three sMMG_{lic} signals, as follows:

$$|sMMG_{lic}| = \sqrt{sMMG_{lic} X^2 + sMMG_{lic} Y^2 + sMMG_{lic} Z^2}$$

oesEMG_{di} and sEMG_{lic} signals were resampled at 2000 Hz, and filtered with a 4th-order zero-phase Butterworth band-pass filter between 5 and 400 Hz and with four 10th-order zero-phase notch filters to remove the power line interference at 50 Hz and its harmonics at 150, 250, and 350 Hz.

Respiratory cycle segmentation and selection. Flow and pressure signals were segmented into inspiratory and expiratory segments by means of a zero-crossing detector on the flow signal, as previously described²⁴. After segmentation all cycles were visually inspected and those either containing artefacts within the EMG and MMG signals or having an unusual P_{di} pattern were rejected. The following parameters were then calculated for each respiratory cycle: inspiratory time, total breath time, and mean P_{di}. The median values of all respiratory cycles during resting breathing and threshold loading were then calculated and 10 cycles that contained the three parameters nearest to the median values were automatically selected, resulting in a total of sixty respiratory cycles for each subject.

P_{di} parameters. The level of inspiratory muscle force during each respiratory cycle was calculated as the mean of the inspiratory P_{di} signal. Transdiaphragmatic pressure-time product (PTP_{di}), the time-integral of P_{di}^{25,26}, was also calculated for each respiratory cycle by multiplying the area under the curve of the inspiratory P_{di} signal by the respiratory frequency, and had units of cmH₂O·s·min⁻¹²⁶. Both mean P_{di} and PTP_{di} parameters were calculated after removal of the baseline from the inspiratory P_{di} signal, which was determined for each respiratory cycle as the minimum level observed from the start of inspiration to the start of expiration (i.e. between points of zero flow).

Quantification of oesEMG_{di} signals using RMS. An additional 4th-order zero-phase Butterworth high-pass filter at 20 Hz was applied to oesEMG_{di} signals in order to reduce the P and T waves of electrocardiographic artefacts, and the low-frequency, large amplitude deflections in signal baseline produced by electrode motion and oesophageal peristalsis²⁷. oesEMG_{di} signals were converted to RMS using a moving window of 50 ms with a one-sample step. The RMS peak values of oesEMG_{di} of a subject's sixty respiratory cycles were then determined by manually analysing inspiratory oesEMG_{di} signal segments falling between QRS complexes of the electrocardiographic noise². For each respiratory cycle, the highest value obtained across all five bipolar electrode pairs was selected (peak RMS oesEMG_{di}). As previously described^{2,9}, the per-breath RMS peak values of oesEMG_{di} were expressed

as percentages of the largest RMS peak value of oesEMG_{di} obtained throughout the inspiratory threshold loading protocol and the three maximal volitional manoeuvres (peak RMS oesEMG_{di%max}).

Quantification of EMG and MMG signals using fSampEn. Sample entropy is a measure of the complexity of a time-series signal²⁸, and depends on the regularity of a signal, so that the higher the regularity, the lower the complexity, and the lower the entropy of a signal. For a given signal, regularity is calculated as the probability given by the ratio A/B , where A and B are the number of pairs of signal segments of length $m + 1$ and m , respectively, that are similar, that is with a maximum sample-by-sample difference less than a predefined tolerance parameter (r). The input parameter m is commonly set at 2 samples. However, r is usually expressed as a function of the standard deviation of the signal analysed. In fSampEn, the sample entropy is calculated within a moving window, instead of over the whole signal, using a fixed r value¹³. In this way, the fSampEn of a signal is a time-series whose values are higher not only when the signal is more complex, but also when the signal includes a wider range of amplitudes.

In this study, the oesEMG_{di}, sEMG_{lic}, and |sMMG_{lic}| signals were converted to fSampEn using a moving window of 750 ms with a 50-ms step and $m = 2$. The tolerance parameter, r , was set at 0.1 and 0.5 times the mean standard deviation EMG and MMG values, respectively, of respiratory cycles of the upper half loads. Values of fSampEn parameters were selected in accordance with the guidelines proposed by Estrada *et al.*²⁹.

The level of inspiratory muscle force and activation during each respiratory cycle was calculated as the mean inspiratory fSampEn of the MMG and EMG signals, respectively.

Analogous to PTP_{di}, a novel index, the “entropy-time product (ETP)”, was calculated by multiplying the area under the curve of the inspiratory fSampEn of the MMG (ETP |sMMG_{lic}|) signals by the respiratory frequency. Thus, ETP had units of $s \cdot \text{min}^{-1}$.

Statistical analysis. All data are expressed as median (interquartile range). Correlation coefficients were determined to measure the relationships between the recorded signals. Normality of all the parameters calculated for each subject was tested using Lilliefors tests. Since not all parameters had a normal distribution, and a linear relationship between them could not be assumed a priori, the degree of association between parameters was measured using Spearman’s rank correlation (ρ). The significance level for all correlations was set at 0.05. Statistical differences in breathing pattern (inspiratory time and respiratory rate), pressures (P_{mo} and P_{di}) and breathlessness (mBorg) between first and last loads of the loading protocol were analysed using non-parametric Wilcoxon signed rank tests.

Within-subject correlation coefficients were calculated over the 60 respiratory cycles of each individual. A group mean correlation coefficient of the 12 participants was also calculated for each pair of parameters using the Fisher z-transform. After applying the Fisher z-transform to the correlation coefficients of the 12 participants, the transformed z-values were averaged, and the inverse Fisher z-transform was applied to the average z-value to convert it back to a group mean correlation coefficient^{30,31}.

The strength of correlation coefficients was interpreted according to Evans’ classification³², where correlation coefficients between 0.2 and 0.39 represent a weak correlation, coefficients between 0.4 and 0.59 represent a moderate correlation, coefficients between 0.6 and 0.79 represent a strong correlation, and coefficients of 0.8 and above represent a very strong correlation.

Results

Twelve subjects (6 male, age 33 (30–38) years, BMI 22.2 (20.6–24.2) kg/m^2 , FEV₁ 98.0 (94.8–105.5) % of predicted, FVC 105.0 (91.5–110.2) % of predicted, FEV₁/FVC 82.0 (74.1–83.9) %) were recruited and completed the incremental inspiratory loading protocol.

Breathing pattern, pressure generation and breathlessness intensity during incremental inspiratory threshold loading. Representative recordings from a single subject during resting breathing and loads 1 to 5 of the inspiratory threshold loading protocol are shown in Fig. 1.

The group median (interquartile range) P_{lmax} was 87.0 (78.0–116.5) cmH_2O equivalent to 109.0 (89.5–126.5) % of predicted values³³. The inspiratory threshold loads increased from 11 (10–14) cmH_2O during load 1 to 52 (47–70) cmH_2O during load 5. P_{mo} increased from 0.3 (0.3–0.4) cmH_2O during resting breathing to 53.7 (49.5–68.4) cmH_2O ($P < 0.001$) at the end of load 5. P_{di} increased from 11.1 (7.1–11.7) cmH_2O at rest to 64.4 (46.1–67.9) cmH_2O ($P < 0.001$) at the end of load 5. Inspiratory time ranged from 1.7 (1.4–2.1) to 2.2 (1.8–2.6) s ($P = 0.11$), and respiratory rate ranged from 13 (11–15) to 12 (10–13) $\text{breaths} \cdot \text{min}^{-1}$ ($P = 0.27$). mBorg breathlessness intensity increased from 0.5 (0.0–0.8) during load 1 to 4.0 (2.5–5.5) by the end of load 5 ($P < 0.001$).

Comparison between RMS and fSampEn for myographic signal analysis. RMS and fSampEn time-series of a representative subject’s myographic signals are shown in Fig. 2.

There was a very strong positive group mean correlation between mean fSampEn oesEMG_{di} and oesEMG_{di%max} ($\rho = 0.81$) (Fig. 3). Individual correlation coefficients are shown in Table 1. All correlations were statistically significant ($P < 0.05$).

The RMS peaks corresponding to cardiac noise were clearly identifiable and greater in the RMS than in the fSampEn time-series (Fig. 2). This was quantified by calculating the level of cardiac noise as the average ratio, in decibels, between the peak value of segments with and without cardiac noise. This ratio was calculated for the expiratory phases of resting breathing and the final load of all RMS and fSampEn time-series shown in Fig. 2 (Table 2).

In light of the strong positive group mean correlation between mean fSampEn oesEMG_{di} and oesEMG_{di%max} and the robustness of fSampEn to cardiac noise, from here on EMG and MMG data will be presented as the mean fSampEn value only.

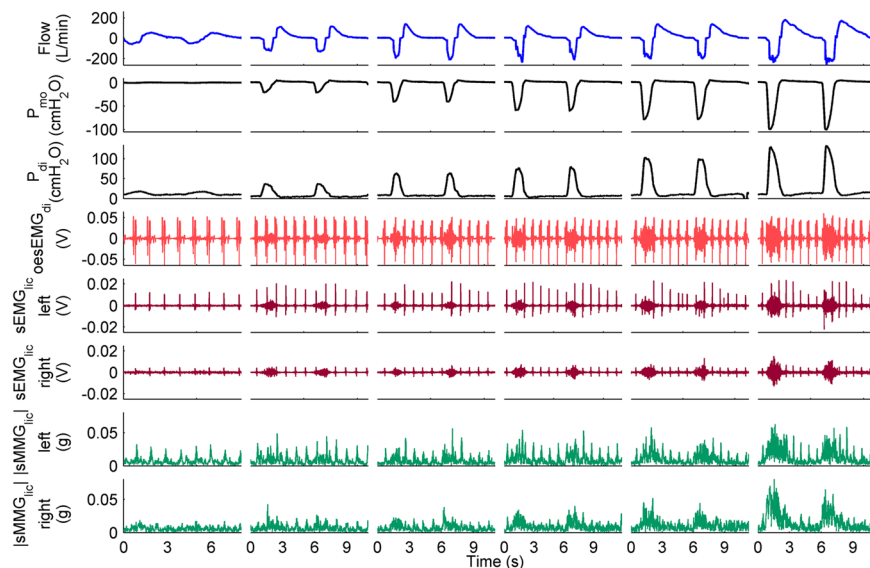


Figure 1. Measurements recorded during the inspiratory threshold loading protocol in a healthy subject. Two respiratory cycles are shown for quiet resting breathing and inspiratory threshold loads equivalent to 12%, 24%, 36%, 48%, and 60% of P_{Imax} (left to right). The oesEMG_{di} signal corresponds to the electrode pair 1.

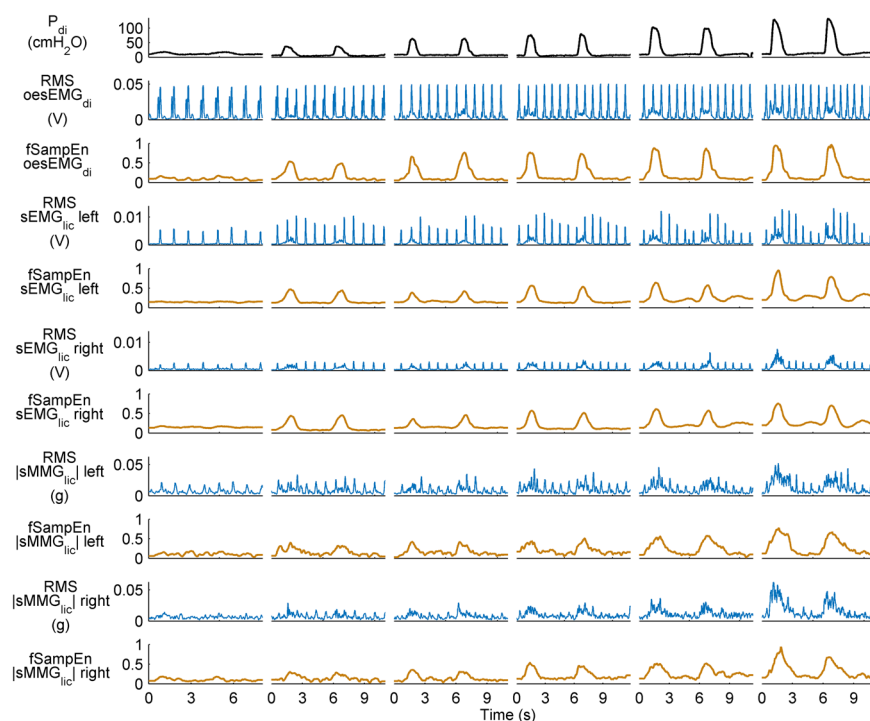


Figure 2. RMS and fSampEn time-series of EMG and MMG signals shown in Fig. 1. Two respiratory cycles are shown for quiet breathing and 12%, 24%, 36%, 48%, and 60% of P_{Imax} (left to right).

Patterns of inspiratory muscle activation during incremental inspiratory threshold loading. In general, mean P_{di}, mean fSampEn sEMG_{lic}, and mean fSampEn |sMMG_{lic}| increased progressively during the inspiratory threshold loading protocol. However, mean fSampEn oesEMG_{di} increased relatively less at higher than at lower loads (Fig. 4).

Mean fSampEn sEMG_{lic} behaved similarly to mean fSampEn oesEMG_{di} up to 36% of P_{Imax}, but continued to increase at inspiratory threshold loads above this level.

Correlations between invasive and non-invasive indices of inspiratory muscle force. Strong to very strong positive group mean correlations were obtained between mean P_{di} and mean fSampEn |sMMG_{lic}|

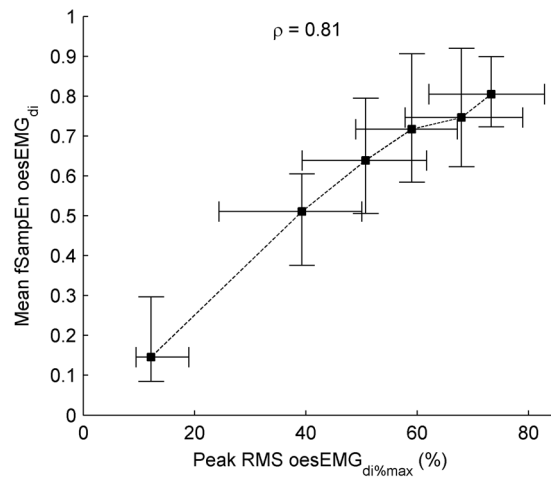


Figure 3. Relationship between RMS- and fSampEn-derived measures of oesEMG_{di}. Data points represent median and interquartile range of the 120 respiratory cycles of the twelve study subjects for each load. The group mean correlation coefficient, ρ , of the twelve subjects was calculated using the Fisher z-transform. Dashed lines show the order of execution of the inspiratory threshold loads.

Subject ID	Spearman's ρ oesEMG _{di\%max} - mean fSampEn oesEMG _{di}
1	0.67
2	0.87
3	0.83
4	0.72
5	0.85
6	0.76
7	0.76
8	0.79
9	0.84
10	0.85
11	0.67
12	0.93
Group mean	0.81

Table 1. Spearman's rank correlation coefficients (ρ) between oesEMG_{di\%max} and mean fSampEn oesEMG_{di}. All correlations were statistically significant ($P < 0.05$).

	oesEMG _{di}	sEMG _{lic} left	sEMG _{lic} right	sMMG _{lic} left	sMMG _{lic} right
RMS at rest	27.16	21.36	13.07	6.56	0.98
RMS at load 5	23.18	20.06	13.11	9.09	3.60
fSampEn at rest	4.05	0.06	0.26	2.20	-0.25
fSampEn at load 5	0.52	-0.52	-0.33	1.06	1.25

Table 2. Level of cardiac noise, in decibels, of the RMS and fSampEn time-series shown in Fig. 2. The average ratio between the peak value of segments with and without cardiac noise was calculated for the expiratory phases.

left ($\rho = 0.76$, Fig. 5a) and right ($\rho = 0.81$, Fig. 5b), and between PTP_{di} and ETP |sMMG_{lic}| left ($\rho = 0.78$, Fig. 5c) and right ($\rho = 0.83$, Fig. 5d). Individual correlation coefficients are shown in Table 3, and individual relationships between mean P_{di} and mean fSampEn |sMMG_{lic}|, and between PTP_{di} and ETP |sMMG_{lic}| are shown in the Supplementary Fig. S1. Individual and group mean correlations between the time-integrals of P_{di} and fSampEn |sMMG_{lic}| signals are shown in the Supplementary Table S1. All correlations were statistically significant ($P < 0.05$). These strong positive group mean correlations were observed despite an increase in the slope of the relationship between mean fSampEn |sMMG_{lic}| and mean P_{di} values at loads L2–L5 relative to loads L0–L2 (Fig. 5a,b, Supplementary Table S2).

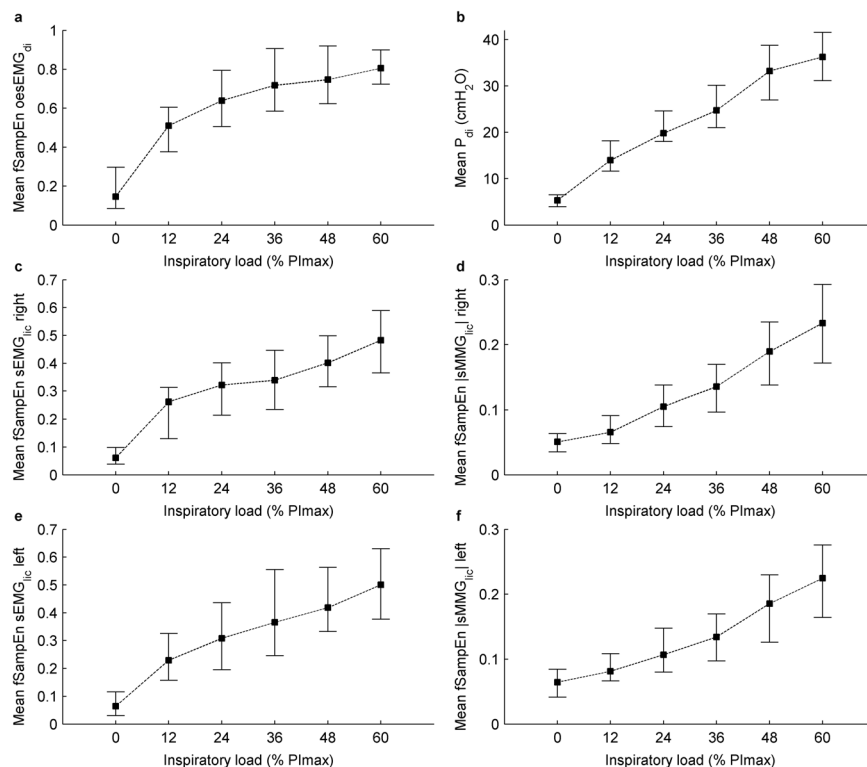


Figure 4. Measures of inspiratory muscle force and activation during inspiratory threshold loading. Data points represent median and interquartile range of the 120 respiratory cycles of the twelve study subjects for each load. Dashed lines show the order of execution of the inspiratory threshold loads.

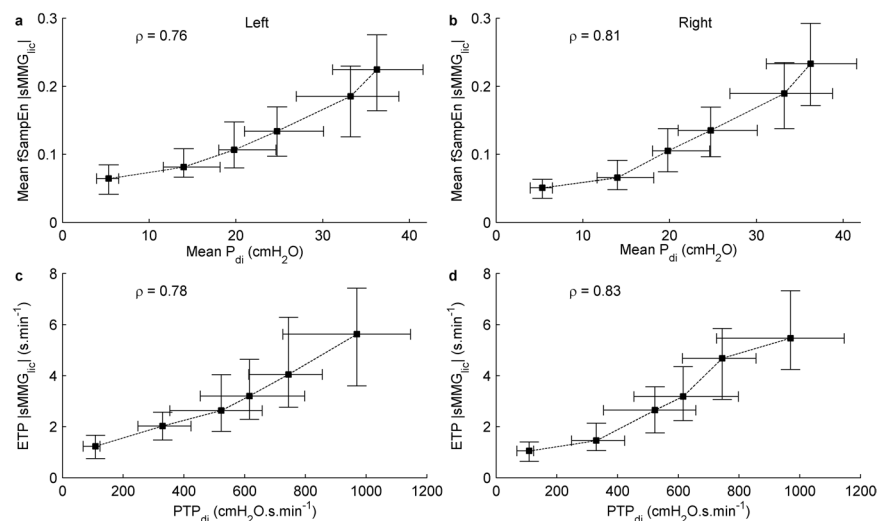


Figure 5. Relationship between invasive and non-invasive measures of inspiratory muscle force output recorded from the left and right sides, calculated as the mean (a,b) and time-integral (c,d) of the P_{di} and $fSampEn |sMMG_{lic}|$ signals. Data points represent median and interquartile range of the 120 respiratory cycles of the twelve study subjects for each load. The group mean correlation coefficients, ρ , of the twelve subjects were calculated using the Fisher z-transform. Dashed lines show the order of execution of the inspiratory threshold loads.

Correlations between invasive oesEMG_{di} and non-invasive sEMG_{lic} measures. Very strong positive group mean correlations were obtained between mean $fSampEn oesEMG_{di}$ and mean $fSampEn sEMG_{lic}$ left ($\rho = 0.84$, Fig. 6a) and right ($\rho = 0.83$, Fig. 6b). Individual correlation coefficients are shown in Table 4. All correlations were statistically significant ($P < 0.05$).

Subject ID	Spearman's ρ Mean P_{di} - Mean fSampEn sMMG _{lic}		Spearman's ρ PTP _{di} - ETP sMMG _{lic}	
	Left	Right	Left	Right
1	0.8	0.88	0.84	0.88
2	0.67	0.87	0.72	0.89
3	0.8	0.78	0.85	0.84
4	0.77	0.79	0.91	0.94
5	0.87	0.9	0.83	0.81
6	0.78	0.72	0.8	0.77
7	0.76	0.9	0.83	0.92
8	0.88	0.82	0.8	0.79
9	0.42	0.57	0.41	0.48
10	0.88	0.81	0.85	0.79
11	0.73	0.75	0.77	0.85
12	0.51	0.72	0.33	0.64
Group mean	0.76	0.81	0.78	0.83

Table 3. Spearman's rank correlation coefficients (ρ) between invasive (P_{di}) and non-invasive (sMMG_{lic}) measures of inspiratory muscle force. Correlations between mean values, and between the corresponding time-integrals (PTP_{di} and ETP |sMMG_{lic}|), are shown. All correlations were statistically significant ($P < 0.05$).

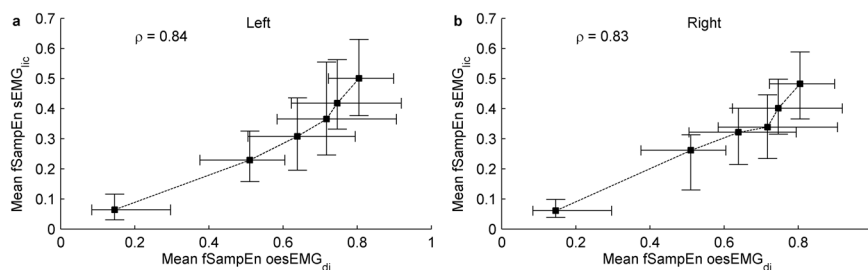


Figure 6. Relationship between invasive and non-invasive measures of inspiratory muscle electrical activation recorded from the left (a) and right (b) sides, calculated as the mean of the fSampEn oesEMG_{di} and sEMG_{lic} signals. Data points represent median and interquartile range of the 120 respiratory cycles of the twelve study subjects for each load. The group mean correlation coefficients, ρ , of the twelve subjects were calculated using the Fisher z-transform. Dashed lines show the order of execution of the inspiratory threshold loads.

Discussion

In this study, sMMG_{lic}, P_{di} , sEMG_{lic} and oesEMG_{di} have been measured simultaneously for the first time, allowing investigation of the relationship between non-invasive and invasive indices of inspiratory muscle force, and electrical activation, respectively. The main finding of this study was the observation of strong to very strong positive correlations between sMMG_{lic}, a novel non-invasive index of inspiratory muscle force output, and the invasive gold standard measure of diaphragm pressure generation, P_{di} . Very strong correlations were also observed between non-invasive sEMG_{lic} and invasive oesEMG_{di} measures. Furthermore, this study is the first to demonstrate strong correlations between RMS- and fSampEn-derived measures of oesEMG_{di}, and, importantly, the superior signal-to-noise ratio of fSampEn over RMS analysis of oesEMG_{di} signals, including attenuation of the cardiac artefact. This supports the use of the fSampEn technique to analyse respiratory muscle electromyogram signals.

The peak force and power output of skeletal muscle depends upon numerous factors, including muscle and fibre size and length, muscle fibre type, force-velocity relationship and the force-frequency relationship³⁴. All of these factors are relevant to respiratory muscle function^{7,35–38}. It is not possible to measure the force produced by the diaphragm muscle directly, and the best index of this force is P_{di} , which can be recorded either during voluntary manoeuvres^{39,40} or in response to phrenic nerve stimulation^{3,40,41}. P_{di} is defined as the difference between intrapleural and abdominal pressure⁴² and, in practice, is generally equated to the arithmetic difference between gastric and oesophageal pressure³. Measurement of P_{di} therefore requires insertion of balloon-catheters^{7,41} or a solid-state dual-pressure transducer tipped catheter²⁰, as used in the present study.

The strong relationship between sMMG_{lic} and P_{di} in the present study suggests that sMMG_{lic} could provide a reliable non-invasive index of inspiratory muscle force output. The MMG signal recorded at the skin surface records the summation of the mechanical activity of single MUs as pressure waves generated by the active muscle fibres, and does not, therefore, provide a direct measure of muscle force. However, the pressure waves generated by muscle fibre activity have been suggested to reflect the mechanical aspects of muscle contraction: the gross lateral movement related to the overall change of muscle geometry at the beginning of contraction, the smaller

Subject ID	Spearman's ρ Mean fSampEn oesEMG _{di} - Mean fSampEn sEMG _{lic}	
	Left	Right
1	0.82	0.83
2	0.87	0.89
3	0.82	0.82
4	0.79	0.81
5	0.82	0.87
6	0.89	0.89
7	0.76	0.67
8	0.86	0.83
9	0.87	0.9
10	0.83	0.84
11	0.85	0.79
12	0.88	0.71
Group mean	0.84	0.83

Table 4. Spearman's rank correlation coefficients (ρ) between invasive (oesEMG_{di}) and non-invasive (sEMG_{lic}) signals. Correlations between mean values are shown. All correlations were statistically significant ($P < 0.05$).

subsequent vibrations at the resonance frequency of the muscle, and the dimensional changes in the active muscle fibres⁴³. As such, sMMG has been extensively evaluated in non-respiratory muscle groups as a tool to investigate MU recruitment strategies^{44,45}, and as indirect indices of muscle function, including muscle force output and fatigability⁴⁶. Studies of locomotor^{47,48}, upper limb^{49–51} and intrinsic hand muscle^{50,52} function, have reported curvilinear relationships between the RMS sMMG and force output expressed as a % of maximum voluntary contraction (%MVC). sMMG has been observed to plateau, or even subsequently decrease, at higher activation levels in a manner that differs from muscle to muscle. Since the amplitude of MMG signals is related to both the tension increase and the velocity of tension increase during twitch and tetanic contractions⁵³, it has been postulated that a decrease in MMG amplitude at higher firing rates reflects fusion of the mechanical activity of MUs in relation to the elevated firing rate^{50,53}. It has therefore been proposed that the variation in RMS-sMMG/%MVC relationships between muscles corresponds to differences in MU activation strategy (MU recruitment vs frequency modulation) due to differences in muscle size and histochemical type⁵⁰. RMS-sMMG/%MVC relationships have also been reported to vary with age⁴⁹, sex⁵¹, and joint angle⁵⁴. Single MU recordings of the diaphragm have previously shown that the diaphragm muscle predominantly employs a strategy of frequency modulation, rather than progressive recruitment of MUs throughout contraction⁵⁵. In this way, the behaviour of the diaphragm is, interestingly, more similar to that of intrinsic hand muscles than that of large proximal muscles⁵⁶. RMS sMMG recordings contributed to by diaphragm muscle fibres alone would therefore be expected to plateau at a relatively low %P_{imax}, akin to RMS-sMMG/%MVC relationships observed in intrinsic hand muscles⁵⁰. In the present study, however, both mean fSampEn sEMG_{lic} and mean fSampEn |sMMG_{lic}|, but not mean fSampEn oesEMG_{di}, increased progressively as %P_{imax} and P_{di} increased, without an observable plateau. The lack of progressive increase in mean fSampEn oesEMG_{di} likely reflects the increasing contribution of extradiaphragmatic muscle activity to non-invasive |sMMG_{lic}| and sEMG_{lic} signals, but not to invasive oesEMG_{di} signals, recorded at the highest inspiratory threshold loads⁵⁷.

Few previous studies have investigated the utility of sMMG in respiratory muscle physiology. Petitjean and Bellemare¹², using condenser microphones, reported significant linear relationships between the amplitude of the right and left phonomyogram and P_{di} peak values, elicited by phrenic nerve stimulation. Recently, Sarlabous *et al.*¹⁵ used uniaxial accelerometers to record sMMG_{lic} in patients with chronic obstructive pulmonary disease and healthy subjects during an incremental inspiratory flow protocol. Very strong correlations were observed between sMMG_{lic} and peak inspiratory P_{mo}. There was also a strong correlation between sMMG_{lic} and FEV₁ in patients, suggesting the potential utility of sMMG_{lic} as a novel non-invasive index of the mechanical load on the respiratory muscles. Distinct to this previous work, the present study employed triaxial accelerometers to record sMMG_{lic}, allowing inspiratory muscle vibrations to be measured in all three spatial directions. Uniaxial accelerometers detect muscle mechanical activity in one spatial direction only and can therefore lead to an underestimation of muscle mechanical activation. Moreover, inspiratory threshold loading allowed the sMMG_{lic} to be measured over a wider range of respiratory effort than the inspiratory flow protocol employed previously by Sarlabous *et al.*¹⁵.

Invasive measurement of P_{di} and oesEMG_{di} is technically complex, requires some skill from the operator involved, may be time-consuming, and most importantly can be uncomfortable for study participants. In this regard, non-invasive techniques would facilitate the assessment of inspiratory muscle force and activation in physiological, and clinical, studies at scale. In contrast to sMMG, sEMG has been used extensively to assess respiratory muscle activation^{17,58–62}. Reilly *et al.*²⁰ reported a very strong correlation between non-invasive parasternal intercostal muscle EMG (sEMG_{para}) and oesEMG_{di} during an incremental cycle exercise test to exhaustion in healthy subjects and in cystic fibrosis patients with chronic airway obstruction. PTP_{di} increased with increasing sEMG_{para} in healthy subjects, whereas PTP_{di} in cystic fibrosis patients plateaued at submaximal oesEMG_{di} and sEMG_{para} levels reflecting neuromechanical uncoupling as a consequence of impaired respiratory mechanics in chronic lung disease. Simultaneous recordings of sEMG_{lic} and sMMG_{lic}, as described in the present study, could therefore

provide the potential to assess the relationships between electrical and mechanical activation of inspiratory muscles in a wholly non-invasive manner. The oesEMG_{di} is increasingly recognized to provide an index of neural respiratory drive which, together with measures of respiratory muscle pressure generation, are facilitating a greater understanding of the neurophysiology of breathlessness perception in health and in respiratory disease^{10,63,64}. sMMG_{lic} and sEMG_{lic} could therefore provide non-invasive estimates of neural respiratory drive to further this work at scale. A combination of sMMG_{lic} and sEMG_{lic} could also provide clinically applicable non-invasive indices of respiratory muscle function that could be particularly useful in the following settings: monitoring of acute exacerbations of chronic obstructive pulmonary disease^{65,66}, weaning from mechanical ventilation in critical care settings⁶⁷, monitoring of diaphragm weakness as a prognostic factor in motor neuron disease¹, and monitoring patients who cannot reliably perform lung function⁶⁸. The increase in the slope of the relationship between the non-invasive measures (sMMG_{lic} and sEMG_{lic}) and invasive measures (P_{di} and oesEMG_{di}) at the highest inspiratory threshold loads, which we suggest is due to increased extradiaphragmatic respiratory muscle activation, occurred at relatively high levels of diaphragm activation (median(IQR) oesEMG_{di%max} was 50.7% (39.3%–61.7% at load L2). This level of oesEMG_{di%max} is higher than the values typically recorded at rest even in severe COPD patients², and approaches end-exercise values in health and in respiratory disease^{10,20,64}. This change in slope is therefore unlikely to significantly limit the utility of these non-invasive correlates of inspiratory muscle activation within typical clinical settings.

A major novel feature of this study is the use of the fSampEn to analyse the simultaneously recorded oesEMG_{di}, sEMG_{lic} and sMMG_{lic} signals. The fSampEn of a signal is a time-series whose values not only depend on the signal amplitude, but also on the signal complexity. Like RMS, fSampEn can track amplitude changes evoked by EMG and MMG activity. However, since cardiac artefacts are much more regular (less complex) than EMG and MMG signals, which are random in nature, fSampEn is less influenced by cardiac artefacts than RMS, as previously described for sMMG_{lic}¹³ and sEMG_{lic} signals¹⁷. In this study, the potential of fSampEn to reduce cardiac artefacts has been shown, for the first time, in oesEMG_{di} signals, which are more affected by cardiac cross-talk than sEMG_{lic} and sMMG_{lic} signals. Based on the advantageous properties of fSampEn, the entropy-time product has been proposed in this study as a new index to measure inspiratory muscle force output from sMMG_{lic} signals. The ETP parameter allows inspiratory muscle activity to be analysed over the whole inspiratory phase of a respiratory cycle regardless of cardiac noise which can be markedly elevated depending on recording site. Accordingly, no relevant differences have been found between correlation values of left and right sides in healthy subjects. However, an RMS-based analysis, which has been the conventional approach to analyse EMG signals, implies prior rejection of signal segments that contain cardiac noise, and therefore provides only coarse estimates of inspiratory muscle activity, since only the RMS peak value of the signal generated during muscle activation is analysed. Moreover, this is a subjective and time-consuming task when performed manually. Although some automatic algorithms have been previously proposed to remove cardiac noise from EMG signals^{69–71}, these algorithms involve the recording of an extra electrocardiographic channel for QRS complexes detection.

Despite the potential for using sMMG_{lic} and sEMG_{lic} to assess inspiratory muscle force and activation non-invasively, we acknowledge limitations of our study, which invites further investigation. Firstly, although our findings suggest that sEMG_{lic} and sMMG_{lic} are useful indices of inspiratory muscle function, these measures are not specific for the diaphragm, since, as discussed above, we cannot exclude the contribution of extradiaphragmatic chest wall and abdominal musculature to these non-invasive signals, particularly during loaded breathing^{72,73}. There is no consensus standard for optimum surface EMG electrode positioning during non-invasive assessment of diaphragm activation, with several recording sites having been suggested for recording electrode placement^{8,59,74–79}. There is also no consensus on methods to maintain electrode orientation with respect to the muscle fibres or to control for the influence of variable muscle-to-electrode distance, such as subcutaneous fat or chest wall deformities that produce variable muscle-to-electrode filtering effects³. The participants in our study cohort were twelve healthy subjects with BMI values within the normal range and the effect of BMI in sMMG_{lic} and sEMG_{lic} measures should therefore be a focus of future research. Future work should also investigate the reproducibility of the sMMG_{lic} measures in health and disease.

Regarding fSampEn, although this parameter tracked amplitude changes of related physiological signals in this and in previous studies^{14,15,17}, fSampEn values have no units and the true physical meaning remains unclear. Therefore, definition of a normal range of values and a normalization process for fSampEn, as that described by Jolley *et al.*² for oesEMG_{di}, is another important area of research.

In summary, we found strong correlations between non-invasive sMMG_{lic} and sEMG_{lic} measures and invasive P_{di} and oesEMG_{di} measures, respectively, in healthy subjects. The strong correlation between sMMG_{lic} and P_{di} suggests that sMMG_{lic} could provide a novel non-invasive correlate of inspiratory muscle force through which to further the study of the physiology, and pathophysiology, of inspiratory muscle function in health and disease.

Data Availability

The datasets analysed during the current study are available from the corresponding author on reasonable request.

References

- Polkey, M. I. *et al.* Respiratory muscle strength as a predictive biomarker for survival in amyotrophic lateral sclerosis. *Am. J. Respir. Crit. Care Med.* **195**, 86–95 (2017).
- Jolley, C. J. *et al.* Neural respiratory drive in healthy subjects and in COPD. *Eur. Respir. J.* **33**, 289–297 (2009).
- American Thoracic Society/European Respiratory Society. ATS/ERS Statement on respiratory muscle testing. *Am. J. Respir. Crit. Care Med.* **166**, 518–624 (2002).
- Sharp, J. T. & Hyatt, R. E. Mechanical and electrical properties of respiratory muscles. In *Handbook of Physiology, The Respiratory System, Mechanics of Breathing* 389–414, <https://doi.org/10.1002/cphy.cp030323> (1986).
- Wade, O. L. Movements of the thoracic cage and diaphragm in respiration. *J. Physiol.* **124**, 193–212 (1954).

6. Mead, J. & Loring, S. H. Analysis of volume displacement and length changes of the diaphragm during breathing. *J. Appl. Physiol.* **53**, 750–5 (1982).
7. Moxham, J., Morris, A. J. R., Spro, S. G., Edwards, R. H. T. & Green, M. Contractile properties and fatigue of the diaphragm in man. *Thorax* **36**, 164–168 (1981).
8. Luo, Y. M. *et al.* Diaphragm electromyogram measured with unilateral magnetic stimulation. *Eur. Respir. J.* **13**, 385–90 (1999).
9. Reilly, C. C. *et al.* Neural respiratory drive measured during inspiratory threshold loading and acute hypercapnia in healthy individuals. *Exp. Physiol.* **98**, 1190–1198 (2013).
10. Jolley, C. J. *et al.* Neural respiratory drive and breathlessness in COPD. *Eur. Respir. J.* **45**, 355–364 (2015).
11. Barry, D. T. Acoustic signals from frog skeletal muscle. *Biophys J* **51**, 769–773 (1987).
12. Petitjean, M. & Bellemare, F. Phonomyogram of the diaphragm during unilateral and bilateral phrenic nerve stimulation and changes with fatigue. *Muscle Nerve* **17**, 1201–1209 (1994).
13. Sarlabous, L., Torres, A., Fiz, J. A. & Jané, R. Evidence towards improved estimation of respiratory muscle effort from diaphragm mechanomyographic signals with cardiac vibration interference using sample entropy with fixed tolerance values. *PLoS One* **9**, e88902 (2014).
14. Sarlabous, L. *et al.* Efficiency of mechanical activation of inspiratory muscles in COPD using sample entropy. *Eur. Respir. J.* **46**, 1808–1811 (2015).
15. Sarlabous, L. *et al.* Inspiratory muscle activation increases with COPD severity as confirmed by non-invasive mechanomyographic analysis. *PLoS One* **12**, e0177730 (2017).
16. Beck, T. W. *et al.* Mechanomyographic amplitude and mean power frequency versus torque relationships during isokinetic and isometric muscle actions of the biceps brachii. *J Electromyogr Kinesiol* **14**, 555–564 (2004).
17. Estrada, L., Torres, A., Sarlabous, L. & Jané, R. Improvement in neural respiratory drive estimation from diaphragm electromyographic signals using fixed sample entropy. *IEEE J. Biomed. Heal. Informatics* **20**, 476–485 (2016).
18. Baydur, A., Behrakis, P. K., Zin, W. A., Jaeger, M. & Milic-Emili, J. A simple method for assessing the validity of the esophageal balloon technique. *Am. Rev. Respir. Dis.* **126**, 788–91 (1982).
19. Watson, A. C. *et al.* Measurement of twitch transdiaphragmatic, esophageal, and endotracheal tube pressure with bilateral anterolateral magnetic phrenic nerve stimulation in patients in the intensive care unit. *Crit. Care Med.* **29**, 1325–31 (2001).
20. Reilly, C. C. *et al.* Neural respiratory drive, pulmonary mechanics and breathlessness in patients with cystic fibrosis. *Thorax* **66**, 240–246 (2011).
21. Luo, Y. M. & Moxham, J. Measurement of neural respiratory drive in patients with COPD. *Respir. Physiol. Neurobiol.* **146**, 165–174 (2005).
22. Chien, M. Y., Wu, Y. T. & Chang, Y. J. Assessment of diaphragm and external intercostals fatigue from surface EMG using cervical magnetic stimulation. *Sensors* **8**, 2174–2187 (2008).
23. Borg, G. A. Psychophysical bases of perceived exertion. *Med. Sci. Sports Exerc.* **14**, 377–81 (1982).
24. Fiz, J. A., Jané, R., Lozano, M., Gómez, R. & Ruiz, J. Detecting unilateral phrenic paralysis by acoustic respiratory analysis. *PLoS One* **9**, e93595 (2014).
25. Marini, J. J., Smith, T. C. & Lamb, V. J. External work output and force generation during synchronized intermittent mechanical ventilation: effect of machine assistance on breathing effort. *Am. Rev. Respir. Dis.* **138**, 1169–1179 (1988).
26. Kyroussis, D. *et al.* Respiratory muscle activity in patients with COPD walking to exhaustion with and without pressure support. *Eur. Respir. J.* **15**, 649–655 (2000).
27. Luo, Y. M., Moxham, J. & Polkey, M. I. Diaphragm electromyography using an oesophageal catheter: current concepts. *Clin. Sci. (Lond.)* **115**, 233–44 (2008).
28. Richman, J. S. & Moorman, J. R. Physiological time-series analysis using approximate entropy and sample entropy. *Am. J. Physiol. Hear. Circ. Physiol.* **278**, 2039–2049 (2000).
29. Estrada, L., Torres, A., Sarlabous, L. & Jané, R. Influence of parameter selection in fixed sample entropy of surface diaphragm electromyography for estimating respiratory activity. *Entropy* **19**, 460 (2017).
30. Corey, D. M., Dunlap, W. P. & Burke, M. J. Averaging correlations: expected values and bias in combined pearson rs and fisher's z transformations. *J. Gen. Psychol.* **125**, 245–261 (1998).
31. Bonett, D. G. & Wright, T. A. Sample size requirements for estimating pearson, kendall and spearman correlations. *Psychometrika* **65**, 23–28 (2000).
32. Evans, J. D. *Straightforward statistics for the behavioral sciences.* (Brooks/Cole, 1996).
33. Wilson, S. H., Cooke, N. T., Edwards, R. H. & Spiro, S. G. Predicted normal values for maximal respiratory pressures in caucasian adults and children. *Thorax* **39**, 535–8 (1984).
34. Fitts, R. H., McDonald, K. S. & Schluter, J. M. The determinants of skeletal muscle force and power: their adaptability with changes in activity pattern. *J. Biomech.* **24**, 111–122 (1991).
35. Rahn, H., Otis, A. B., Chadwick, L. E. & Fenn, W. O. The pressure-volume diagram of the thorax and lung. *Am J Physiol* **146**, 161–178 (1946).
36. Pengelly, L. D., Alderson, A. M. & Milic-Emili, J. Mechanics of the diaphragm. *J Appl Physiol* **30**, 797–805 (1971).
37. McCully, K. K. & Faulkner, J. A. Length-tension relationship of mammalian diaphragm muscles. *J Appl Physiol* **54**, 1681–1686 (1983).
38. Mier, A., Brophy, C., Moxham, J. & Green, M. Influence of lung volume and rib cage configuration on transdiaphragmatic pressure during phrenic nerve stimulation in man. *Respir Physiol* **80**, 193–202 (1990).
39. Miller, J. M., Moxham, J. & Green, M. The maximal sniff in the assessment of diaphragm function in man. *Clin Sci* **69**, 91–96 (1985).
40. Lyall, R. A., Donaldson, N., Polkey, M. I., Leigh, P. N. & Moxham, J. Respiratory muscle strength and ventilatory failure in amyotrophic lateral sclerosis. *Brain* **124**, 2000–2013 (2001).
41. Steier, J. *et al.* The value of multiple tests of respiratory muscle strength. *Thorax* **62**, 975–80 (2007).
42. Agostoni, E. & Rahn, H. Abdominal and thoracic pressures at different lung volumes. *J Appl Physiol* **15**, 1087–1092 (1960).
43. Cè, E., Rampichini, S. & Esposito, F. Novel insights into skeletal muscle function by mechanomyography: from the laboratory to the field. *Sport Sci. Health* **11**, 1–28 (2015).
44. Beck, T. W. *et al.* Does the frequency content of the surface mechanomyographic signal reflect motor unit firing rates? A brief review. *J Electromyogr Kinesiol* **17**, 1–13 (2007).
45. Malek, M. H. & Coburn, J. W. The utility of electromyography and mechanomyography for assessing neuromuscular function: a noninvasive approach. *Phys. Med. Rehabil. Clin. N. Am.* **23**, 23–32 (2012).
46. Islam, M. A., Sundaraj, K., Ahmad, R. B. & Ahamed, N. U. Mechanomyogram for muscle function assessment: a review. *PLoS One* **8**, e58902 (2013).
47. Miyamoto, N. & Oda, S. Mechanomyographic and electromyographic responses of the triceps surae during maximal voluntary contractions. *J. Electromyogr. Kinesiol.* **13**, 451–459 (2003).
48. Ryan, E. D. *et al.* Mechanomyographic amplitude and mean power frequency responses during isometric ramp vs. step muscle actions. *J. Neurosci. Methods* **168**, 293–305 (2008).
49. Kumi, A., Katsumi, M., Makoto, W. & Kunihiro, I. Age-related change in motor unit activation strategy in force production: a mechanomyographic investigation. *Muscle Nerve* **25**, 505–512 (2002).
50. Akataki, K., Mita, K., Watakabe, M. & Itoh, K. Mechanomyographic responses during voluntary ramp contractions of the human first dorsal interosseous muscle. *Eur. J. Appl. Physiol.* **89**, 520–525 (2003).

51. Nonaka, H., Mita, K., Akataki, K., Watakube, M. & Itoh, Y. Sex differences in mechanomyographic responses to voluntary isometric contractions. *Med. Sci. Sport. Exerc.* **38**, 1311–1316 (2006).
52. Esposito, F. *et al.* Electrical and mechanical response of finger flexor muscles during voluntary isometric contractions in elite rock-climbers. *Eur. J. Appl. Physiol.* **105**, 81 (2008).
53. Bichler, E. Mechanomyograms recorded during evoked contractions of single motor units in the rat medial gastrocnemius muscle. *Eur J Appl Physiol* **83**, 310–319 (2000).
54. Miyamoto, N. & Oda, S. Effect of joint angle on mechanomyographic amplitude during unfused and fused tetani in the human biceps brachii muscle. *Eur. J. Appl. Physiol.* **95**, 221–228 (2005).
55. Gandevia, S. C., Gorman, R. B., McKenzie, D. K. & De Troyer, A. Effects of increased ventilatory drive on motor unit firing rates in human inspiratory muscles. *Am. J. Respir. Crit. Care Med.* **160**, 1598–1603 (1999).
56. De Luca, C. J., LeFever, R. S., McCue, M. P. & Xenakis, A. P. Behaviour of human motor units in different muscles during linearly varying contractions. *J Physiol* **329**, 113–128 (1982).
57. Laghi, F., Topeli, A. & Tobin, M. J. Does resistive loading decrease diaphragmatic contractility before task failure? *J. Appl. Physiol.* **85**, 1103–1112 (1998).
58. Maarsingh, E. J. W., van Eykern, L. A., Sprickelman, A. B., Hoekstra, M. O. & van Aalderen, W. M. C. Respiratory muscle activity measured with a noninvasive EMG technique: technical aspects and reproducibility. *J. Appl. Physiol.* **88**, 1955–1961 (2000).
59. Duiverman, M. L. *et al.* Reproducibility and responsiveness of a noninvasive EMG technique of the respiratory muscles in COPD patients and in healthy subjects. *J. Appl. Physiol.* **96**, 1723–1729 (2004).
60. Glerant, J. C. *et al.* Diaphragm electromyograms recorded from multiple surface electrodes following magnetic stimulation. *Eur. Respir. J.* **27**, 334–42 (2006).
61. Hawkes, E. Z., Nowicky, A. V. & McConnell, A. K. Diaphragm and intercostal surface EMG and muscle performance after acute inspiratory muscle loading. *Respir. Physiol. Neurobiol.* **155**, 213–9 (2007).
62. Wu, W. *et al.* Correlation and compatibility between surface respiratory electromyography and transesophageal diaphragmatic electromyography measurements during treadmill exercise in stable patients with COPD. *Int. J. Chron. Obstruct. Pulmon. Dis.* **12**, 3273–3280 (2017).
63. Jolley, C. J. & Moxham, J. Dyspnea intensity: a patient-reported measure of respiratory drive and disease severity. *Am. J. Respir. Crit. Care Med.* **193**, 236–238 (2016).
64. Faisal, A. *et al.* Common mechanisms of dyspnea in chronic interstitial and obstructive lung disorders. *Am. J. Respir. Crit. Care Med.* **193**, 299–309 (2016).
65. Murphy, P. B. *et al.* Neural respiratory drive as a physiological biomarker to monitor change during acute exacerbations of COPD. *Thorax* **66**, 602–608 (2011).
66. Suh, E.-S. *et al.* Neural respiratory drive predicts clinical deterioration and safe discharge in exacerbations of COPD. *Thorax* **70**, 1123–30 (2015).
67. Harikumar, G. *et al.* Tension–Time Index as a Predictor of Extubation Outcome in Ventilated Children. *Am. J. Respir. Crit. Care Med.* **180**, 982–988 (2009).
68. MacBean, V. *et al.* Parasternal intercostal electromyography: a novel tool to assess respiratory load in children. *Pediatr. Res.* **80**, 407–414 (2016).
69. Sinderby, C., Lindström, L. & Grassino, A. E. Automatic assessment of electromyogram quality. *J. Appl. Physiol.* **79**, 1803–15 (1995).
70. Sinderby, C. A., Beck, J. C., Lindström, L. H. & Grassino, A. E. Enhancement of signal quality in esophageal recordings of diaphragm EMG. *J. Appl. Physiol.* **82**, 1370–1377 (1997).
71. Beck, J., Sinderby, C., Lindström, L. & Grassino, A. Effects of lung volume on diaphragm EMG signal strength during voluntary contractions. *J. Appl. Physiol.* **85**, 1123–1134 (1998).
72. Sinderby, C., Friberg, S., Comtois, N. & Grassino, A. Chest wall muscle cross talk in canine costal diaphragm electromyogram. *J Appl Physiol* **81**, 2312–2327 (1996).
73. Luo, Y. M. *et al.* Diaphragm EMG measured by cervical magnetic and electrical phrenic nerve stimulation. *J Appl Physiol* **85**, 2089–2099 (1998).
74. MacLean, I. C. & Mattioni, T. A. Phrenic nerve conduction studies: a new technique and its application in quadriplegic patients. *Arch Phys Med Rehabil* **62**, 70–73 (1981).
75. Chen, R., Collins, S., Remtulla, H., Parkes, A. & Bolton, C. F. Phrenic nerve conduction study in normal subjects. *Muscle Nerve* **18**, 330–335 (1995).
76. Mills, G. H. *et al.* Unilateral magnetic stimulation of the phrenic nerve. *Thorax* **50**, 1162–72 (1995).
77. Mills, G. H. *et al.* Bilateral magnetic stimulation of the phrenic nerves from an anterolateral approach. *Am J Respir Crit Care Med* **154**, 1099–1105 (1996).
78. Laghi, F., Harrison, M. J. & Tobin, M. J. Comparison of magnetic and electrical phrenic nerve stimulation in assessment of diaphragmatic contractility. *J. Appl. Physiol.* **80**, 1731–42 (1996).
79. Demoule, A., Verin, E., Locher, C., Derenne, J. P. & Similowski, T. Validation of surface recordings of the diaphragm response to transcranial magnetic stimulation in humans. *J Appl Physiol* **94**, 453–461 (2003).

Acknowledgements

Dr. Manuel Lozano-García was the recipient of a European Respiratory Society Fellowship (ERS LTRF 2015-5185). This work was supported by the Government of Catalonia through the CERCA Programme, the Spanish Ministry of Economy and Competitiveness through the project DPI2015-68820-R (MINECO/FEDER), and the Biomedical Research Networking Centre in Bioengineering, Biomaterials and Nanomedicine (CIBER-BBN) (Instituto de Salud Carlos III/FEDER). The funders had no role in study design, data collection and analysis, decision to publish, or preparation of the manuscript.

Author Contributions

M.L.G., J.M., R.J., G.F.R., and C.J.J. contributed to the concept and design of the study; M.L.G., L.S., and C.J.J. performed experiments and collected the data; M.L.G. and L.S. analysed the data and prepared figures; M.L.G. drafted the manuscript; C.J.J. and R.J. reviewed the original draft; All authors interpreted the results, revised and edited the manuscript, commented critically, and approved the final version of the manuscript for submission.

Additional Information

Supplementary information accompanies this paper at <https://doi.org/10.1038/s41598-018-35024-z>.

Competing Interests: The authors declare no competing interests.

Publisher's note: Springer Nature remains neutral with regard to jurisdictional claims in published maps and institutional affiliations.



Open Access This article is licensed under a Creative Commons Attribution 4.0 International License, which permits use, sharing, adaptation, distribution and reproduction in any medium or format, as long as you give appropriate credit to the original author(s) and the source, provide a link to the Creative Commons license, and indicate if changes were made. The images or other third party material in this article are included in the article's Creative Commons license, unless indicated otherwise in a credit line to the material. If material is not included in the article's Creative Commons license and your intended use is not permitted by statutory regulation or exceeds the permitted use, you will need to obtain permission directly from the copyright holder. To view a copy of this license, visit <http://creativecommons.org/licenses/by/4.0/>.

© The Author(s) 2018